



University of
New Haven

University of New Haven
Digital Commons @ New Haven

Mathematics Faculty Publications

Mathematics

2006

Monte Carlo Random Walk Simulations Based on Distributed Order Differential Equations with Applications in Cell Biology

Erik Andries

University of New Mexico

Sabir Umarov

University of New Haven, sumarov@newhaven.edu

Stanly Steinberg

University of New Mexico

Follow this and additional works at: <https://digitalcommons.newhaven.edu/mathematics-facpubs>



Part of the [Mathematics Commons](#)

Publisher Citation

Andries, Erik & Umarov, Sabir & Steinberg, Stanly. (2006). Monte Carlo random walk simulations based on distributed order differential equations with applications to cell biology. *Fractional Calculus and Applied Analysis*, 9(4), 351–369.

Comments

This is the article published in *Fractional Calculus and Applied Analysis*. The original posting is found at <https://eudml.org/doc/11288>.

MONTE CARLO RANDOM WALK SIMULATIONS BASED
ON DISTRIBUTED ORDER DIFFERENTIAL EQUATIONS
WITH APPLICATIONS TO CELL BIOLOGY

Erik Andries ^{†,‡}, Sabir Umarov ^{†,*}, Stanly Steinberg [†]

Abstract

In this paper the multi-dimensional Monte-Carlo random walk simulation models governed by distributed fractional order differential equations (DODEs) and multi-term fractional order differential equations are constructed. The construction is based on the discretization leading to a generalized difference scheme (containing a finite number of terms in the time step and infinite number of terms in the space step) of the Cauchy problem for DODE. The scaling limits of the constructed random walks to a diffusion process in the sense of distributions is proved.

Mathematics Subject Classification: 65C05, 60G50, 39A10, 92C37

Key Words and Phrases: random walk, anomalous diffusion, confined diffusion, distributed order differential equation, Monte-Carlo simulation

1. Introduction

1.1. Motivation. In this paper we study simulation models based on distributed order differential equations, which we call DODE simulations. This type of simulation reflects the rich structure of diffusion media, in which a several diffusion modes are possible. Diffusion processes with complex and changing modes are ubiquitous in nature (see, [2, 5, 18, 22, 26] and references therein). One of the motivations for conducting DODE simulations is to model the movement of proteins on the cell membrane. Numerous

experiments [8, 9, 13, 20, 21] show that macromolecule movement through the cell membrane is distinct from Brownian motion. Saxton and Jacobson [21] noted that practically all experimental results show apparent transitions among modes of motion.

The governing equation, which we take as a basis for our simulation models, in general form, is distributed space fractional order differential equation

$$D_*^\beta u(t, x) = \int_0^2 a(\alpha) D_0^\alpha u(t, x) d\alpha, \quad t > 0, \quad x \in \mathbb{R}^N, \quad (1)$$

where $0 < \beta \leq 1$, D_*^β is the Caputo fractional order derivative [3, 10], $D_0^\alpha = (-\Delta)^{\frac{\alpha}{2}}$ is the space fractional order (pseudo-differential) operator with the symbol $|\xi|^\alpha$. Note that D_0^α can be written in the form of hyper-singular integral as well, [19]. The function $a(\alpha)$ is a positive integrable function (or positively defined distribution). Depending on $a(\alpha)$, (1) may become a multi-term fractional order differential equation, which can possibly describe the existence of a finite number of diffusion regimes. Although, the distributed order differential operators were first mentioned by [3, 4] in the 1960s, the intensive study of models based on the distributed order differential equations has been started recently [1, 5, 7, 15, 16, 24, 25].

The present paper is organized as follows. In Section 2, we briefly recall the theoretic platform of the construction of the DODE simulation models announced in [25]. In Section 3 we analyze the difference schemes associated with the DODE models. These difference schemes contain a finite number of terms in the time step and an infinite number of terms in the space step. In the one-dimensional case the analogous schemes are considered in [11, 14]. In Sections 4 and 5 we construct random walk models and simulations based on the transition probabilities introduced in the previous sections.

1.2. Notation. In this paper, \mathbb{R}^N is the N -dimensional Euclidean space with coordinates $x = (x_1, \dots, x_N)$ while Z^N is the N -dimensional integer-valued lattice with the lattice nodes being given by the multi-index notation $j = (j_1, \dots, j_N)$. The letters i, j and k will be exclusively used for the multi-indexing of lattice nodes. We denote by $x_j = (h_{j_1}, \dots, h_{j_N}), j \in Z^N$, the nodes of the uniform h -lattice Z_h^N which is defined as $(hZ)^N$ with h being the distance between any two closest lattice nodes. We introduce a spatial grid $\{x_j = jh, j \in Z^N\}$, with $h > 0$ and a temporal grid $\{t_n = n\tau, n = 0, 1, 2, \dots\}$ with a fixed stepsize $\tau > 0$. Furthermore, let u_j^n denote the discretization of the function $u(t, x)$ on the spatial and temporal grid at $x = x_j$ and $t = t_n$, i.e. $u_j^n = u(t_n, x_j)$.

2. Markovian random walks associated with the DODE

2.1. Particle jumps. Assume \mathbf{X} to be a N -dimensional random vector [17] whose values range in Z^N . Let a sequence of random vectors $\mathbf{X}_1, \mathbf{X}_2, \dots$ also be N -dimensional independent identically distributed random vectors, all having the same probability distribution coinciding with the probability distribution of X . Consider the sequence of random vectors

$$\mathbf{S}_n = h\mathbf{X}_1 + h\mathbf{X}_2 + \dots + h\mathbf{X}_n, n = 1, 2, \dots$$

taking $\mathbf{S}_0 = \mathbf{0} = (0, \dots, 0) \in Z_h^N$, for convenience. We interpret $\mathbf{X}_1, \mathbf{X}_2, \dots$, as a sequence of particle jumps with the starting time $t = t_0 = 0$. At time $t = t_n$, the particle takes a jump $h\mathbf{X}_n$ from \mathbf{S}_{n-1} to \mathbf{S}_n . If $u_j^n = u(t_n, x_j)$ is the probability of a particle being at location x_j at time t_n , then taking into account the recursion $\mathbf{S}_{n+1} = \mathbf{S}_n + h\mathbf{X}_{n+1}$, we have

$$u_j^{n+1} = \sum_{k \in Z^N} p_k u_{j-k}^n, j \in Z^N, n = 0, 1, \dots, \tag{2}$$

where the coefficients $p_k, k \in Z^N$, are called the transition probabilities. The convergence of the sequence \mathbf{S}_n when $n \rightarrow \infty$ means convergence of the discrete probability law (probability mass function) $(u_j^n)_{j \in Z^N}$, properly rescaled as explained below, to the probability law with a density $u(t, x)$ in the sense of distributions (in law). This is equivalent to the locally uniform convergence of the corresponding characteristic functions (see for details [17]). This idea is used in [23, 25] to prove the convergence of the sequence of characteristic functions of the corresponding random walks to the characteristic function of a limit random variable, whose density function is the fundamental solution of a distributed order differential equation.

2.1. Markovian transition probabilities. Let the transition probabilities in Eq.(2) take the form

$$p_k = \tau q_k(h), k \neq 0, \tag{3}$$

where

$$q_k(h) = \int_0^2 \left[\frac{a(\alpha)b(\alpha)}{|k|^{N+\alpha}h^\alpha} \right] d\alpha, \text{ and } b(\alpha) = \frac{[\Gamma(1 + \frac{\alpha}{2})]^2 \sin(\frac{\alpha}{2}\pi)}{\pi^2 2^{N-\alpha-1}}. \tag{4}$$

The transition probability p_0 can then be defined as

$$p_0 = 1 - \sum_{k \neq 0} p_k = 1 - \tau q_0(h), \tag{5}$$

where

$$q_0(h) = \sum_{k \neq 0} q_k(h) = \sum_{k \neq 0} \int_0^2 \left[\frac{a(\alpha)b(\alpha)}{|k|^{N+\alpha}h^\alpha} \right] d\alpha. \quad (6)$$

Assuming that the condition $0 < \tau q_0(h) \leq 1$ is fulfilled, the transition probabilities then satisfy the following properties:

1. $\sum_{k \in Z^N} p_k = 1$;
2. $p_k \geq 0, k \in Z^N$.

Note that the non-negativity condition¹ in property 2 is linked with the Riemann zeta-function. Indeed, introduce the function

$$\mathcal{R}(\alpha) = \sum_{k \neq 0} \frac{1}{|k|^{N+\alpha}} = \sum_{m=1}^{\infty} \frac{M_m}{m^{N+\alpha}}, \quad 0 < \alpha \leq 2, \quad (7)$$

where $M_m = \sum_{|k|=m} 1$. In the one-dimensional case $\mathcal{R}(\alpha) = 2\zeta(1 + \alpha)$, where $\zeta(z)$ is the Riemann zeta-function. Then the condition $0 \leq p_0 \leq 1$ can be rewritten as

$$\tau q_0(h) = \tau \int_0^2 \left[\frac{a(\alpha)b(\alpha)\mathcal{R}(\alpha)}{h^\alpha} \right] d\alpha \leq 1. \quad (8)$$

It follows from this condition that $h \rightarrow 0$ yields $\tau \rightarrow 0$. This, in turn, yields $t/\tau \rightarrow \infty$ for any finite t .

THEOREM 1. *Let \mathbf{X} be a random vector with the transition probabilities $p_k = P(\mathbf{X} = x_k), k \in Z^N$, defined in (3)-(6) which satisfy properties 1 and 2. Then the sequence of random vectors $\mathbf{S}_n = h\mathbf{X}_1 + \dots + h\mathbf{X}_n$ converges as $n \rightarrow \infty$ in law to the random vector whose probability density function is the fundamental solution of the distributed space fractional order differential equation (1) with $\beta = 1$.*

Note, for the simulations used in this paper, it is important to use the multi-term analog of this theorem. Assuming that

$$a(\alpha) = \sum_{m=1}^M a_m \delta(\alpha - \alpha_m), \quad 0 < \alpha_1 < \dots < \alpha_M \leq 2, \quad (9)$$

¹This condition is equivalent to the stability condition of finite-difference schemes giving the usual stability condition if $a(\alpha) = \delta(\alpha - 2)$.

with positive constants a_m , we get a multiterm DODE

$$D_*^\beta u(t, x) = \sum_{m=1}^M a_m D_0^{\alpha_m} u(t, x), \quad t > 0, x \in \mathbb{R}^N. \quad (10)$$

Also note that the coefficients $q_k(h)$ in Eq.(4) and Eq.(6) become multi-term as well:

$$q_k(h) = \sum_{m=1}^M \left[\frac{a_m b(\alpha_m)}{|k|^{N+\alpha_m} h^{\alpha_m}} \right], \quad k \neq 0, \quad q_0 = \sum_{k \neq 0} q_k(h). \quad (11)$$

THEOREM 2. *Let the transition probabilities $p_k = P(\mathbf{X} = x_k), k \in Z^N$, of the random vector \mathbf{X} be given as follows:*

$$p_k = \tau q_k(h) \quad \text{and} \quad p_0 = 1 - \tau q_0(h) \quad (12)$$

where $q_k(h), k \in Z^N$, is defined in (11). Moreover, assume

$$\tau \sum_{m=1}^M \frac{a_m b(\alpha_m) \mathcal{R}(\alpha_m)}{h^{\alpha_m}} \leq 1.$$

Then the sequence of random vectors $\mathbf{S}_n = h\mathbf{X}_1 + \dots + h\mathbf{X}_n$ converges as $n \rightarrow \infty$ in law to the random vector whose probability density function is the fundamental solution of the multiterm fractional order differential equation (10) with $\beta = 1$.

REMARK 1. As we noted above these results were announced in [25]. Theoretically the more general case of these theorems corresponding to a fractional $\beta \in (0, 1)$ can be obtained introducing a positive waiting time distribution and corresponding iid random variables [11, 16]. However, in this paper for the study of the fractional case we apply the numerical approach using general explicit difference schemes with a finite number of terms in the time step and an infinite number of terms in the space step. The obtained difference schemes are stable under some condition and has a unique solution.

3. Generalized transition probabilities for the DODE

The set of grid points in Z_h^N used to update u at time $t = t_{n+1} = (n+1)\tau$ is called the *stencil*. In this section, we start from stating the values of the transition probabilities associated with the stencil for the discretization of the particular space-time-fractional differential equation,

$$D_*^\beta u(t, x) = D_0^\alpha u(t, x), \quad t > 0, x \in \mathbb{R}^N, 0 < \beta \leq 1, 0 < \alpha \leq 2, \quad (13)$$

and then generalize it to distributed order differential equations.

3.1. Discretization of the time-fractional derivative. Using the Caputo time-fractional derivative [3], the left-hand-side of (13) becomes

$$D_*^\beta u(t, x) = \frac{1}{\Gamma(1-\beta)} \int_0^t \left[\frac{\partial u(s, x)}{\partial s} \right] \frac{ds}{(t-s)^\beta}, \quad 0 < \beta < 1. \quad (14)$$

Note that when $\beta = 1$, $D_*^\beta u(t, x) = \partial u / \partial t$. When $0 < \beta < 1$, we will use the following discretization (see [14] for the derivation):

$$\begin{aligned} D_*^\beta u_j^n &\approx \frac{1}{\Gamma(1-\beta)} \sum_{m=0}^n \int_{t_n}^{t_{n+1}} \frac{u_j'(t_{n+1}-s)}{s^\beta} ds \\ &= \frac{1}{\nu \tau^\beta} \left(u_j^{n+1} - \sum_{m=1}^n c_m u_j^{n+1-m} - \gamma_n u_j^0 \right), \end{aligned} \quad (15)$$

where

$$\gamma_m = (m+1)^{1-\beta} - m^{1-\beta}, \quad m = 0, 1, \dots, n, \quad c_m = \gamma_{m-1} - \gamma_m, \quad m = 1, \dots, n,$$

and $\nu = \Gamma(2-\beta)$. The formulas for the coefficients c_m and γ_m and the scalar ν that were used in (15), which were based upon the Caputo time-fractional derivative, easily generalize to other definitions of the time-fractional derivative. For example, in the case of the Grunwald-Letnikov time-fractional derivative, $\nu = 1$ and γ_m and c_m are re-defined as the following [6]:

$$c_m = \left| \binom{\beta}{m} \right|, \quad m = 1, \dots, n, \quad \gamma_m = 1 - \sum_{i=1}^m c_i, \quad m = 0, \dots, n.$$

For simplicity of notation, we will now set

$$\begin{aligned} w_0 &= \gamma_n \\ w_i &= c_{n-i+1}, \quad i = 1, \dots, n, \end{aligned}$$

and, as a result, (15) can be rewritten as

$$D_*^\beta u_j^n = \frac{1}{\nu \tau^\beta} \left(u_j^{n+1} - \sum_{m=0}^n w_m u_j^m \right). \quad (16)$$

Note that for $\beta = 1, \nu = \Gamma(2-\beta) = 1$ and $w_0 = \dots = w_{n-1} = 0$ with $w_n = 1$. In this case, (15) reduces to the standard forward-time discretization for $\partial u/\partial t$:

$$D_*^1 u_j^n = \frac{\partial u}{\partial t} \approx \frac{u_j^{n+1} - u_j^n}{\tau}.$$

3.2. Discretization of the space-fractional derivative. Just as the discretization for the time-fractional derivative assumes a simple form when $\beta = 1$, the discretization for the space-fractional derivative, based upon centered differences, assumes a simple form when $\alpha = 2$. For example, when $\alpha = 2$ and the $N = 2$,

$$D_0^\alpha u_j^n = \Delta u_j^n \approx \frac{1}{h^2} \left(u_{(j_1+1, j_2)}^n + u_{(j_1-1, j_2)}^n + u_{(j_1, j_2+1)}^n + u_{(j_1, j_2-1)}^n - 4u_{(j_1, j_2)}^n \right).$$

In N -dimensions, the stencil consists of the point $x_j, j = (j_1, \dots, j_N)$ and its nearest $2N$ neighbors with each nearest neighbor being h units away from x_j . For a collection of fractional derivative orders $\{\alpha_1, \dots, \alpha_M\}, 0 < \alpha_1 < \dots < \alpha_M < 2$, the right hand side of (10) is given by [25]:

$$\approx -q_0(h)u_j^n + \sum_{k \neq 0} q_k(h)u_{j-k}^n, \tag{17}$$

where the coefficients $q_0(h)$ and $q_k(h)$ are defined in (4) and (6) using the multiterm definition of DODE with $a(\alpha)$. The geometric consequence of changing α from $\alpha = 2$ to $\alpha \neq 2$ or a multiterm DODE is that the stencil gets enlarged from $2N + 1$ grid points to all of the lattice points in Z_h^N .

3.3. Construction of the generalized explicit difference scheme.

Setting the discretizations for the time and space-fractional derivatives equal to each other in (15) and (17), we get

$$\frac{1}{\nu\tau^\beta} \left(u_j^{n+1} - \sum_{m=0}^n w_m u_j^m \right) = -q_0(h)u_j^n + \sum_{k \neq 0} q_k(h)u_{j-k}^n. \tag{18}$$

Solving for u_j^{n+1} , the following *generalized explicit difference scheme*, with a finite difference terms in the time step and an infinite difference terms in the space step, is constructed:

$$u_j^{n+1} = \sum_{m=0}^{n-1} w_m u_j^m + \sum_{k \in Z^N} p_k u_{j-k}^n, \tag{19}$$

where

$$p_k = \nu\tau^\beta q_k(h), \quad k \neq 0 \quad \text{and} \quad p_0 = w_n - \nu\tau^\beta q_0(h).$$

When $\beta = 1$, the coefficients p_k are equivalent to the transition probabilities p_k in (12). Furthermore, since all the transition probabilities are non-negative and taking into account that $w_n = c_1 = 2 - 2^{1-\beta}$ and $\nu = \Gamma(2 - \beta)$, we have an upper bound for the stepsize τ :

$$p_0 \geq 0 \quad \Rightarrow \quad 0 < \tau \leq \left(\frac{2 - 2^{1-\beta}}{\Gamma(2 - \beta)q_0(h)} \right)^{1/\beta}.$$

The update u_j^{n+1} in (19) is determined by Markovian contributions (those values of u at time $t = t_n$) and non-Markovian contributions (those values of u at times $t = \{t_0, t_1, \dots, t_{n-1}\}$). The order of the time fractional derivative β determines the effect that the non-Markovian transition probabilities (w_0, \dots, w_{n-1}) has on u_j^{n+1} . This effect can be measured by examining the sum of all of the transition probabilities in (19):

$$\sum_{m=0}^{n-1} w_m + \sum_{k \in Z^N} p_k = 1, \quad \begin{cases} \sum_{m=0}^{n-1} w_m = 1 - w_n \\ \sum_{k \in Z^N} p_k = w_n. \end{cases} \quad (20)$$

Recall that when $\beta = 1$, $w_n = 1$ and $w_0 = \dots = w_{n-1} = 0$. In this case, the first term in (20) vanishes and $p_0 = 1 - \tau q_0(h)$.

When $0 < \beta < 1$, the values of u_j^n associated with $t \in \{t_0, \dots, t_{n-1}\}$ are weighted by the coefficients $\{w_0, w_1, \dots, w_{n-1}\}$. Figure 1 plots w_m for $m = 0, 1, \dots, n$ where $n = 100$ and $\beta = 0.8$. It is well-known that the sequence $\{w_m\}_{m=1}^n$ are monotone increasing [6], i.e. $w_1 < w_2 < \dots < w_{n-1} < w_n$. However, it is not true $w_0 < w_1$. In fact, in Figure 1, $w_{94} < w_0 < w_{95}$ for both Grunwald-Letnikov and Caputo time-fractional derivative cases. Hence, the contribution of u_j^0 to u_j^{101} is quite large relative to the other intermediate values of u_j^n . We will see later on that this will have important consequences in non-Markovian random walk numerical simulations.

4. Monte Carlo protocol for the random walk

4.1. General framework. The random walk model corresponding to the governing equation in (13) uses the non-Markovian transition probabilities, w_m , and the Markovian transition probabilities, p_k to assign where in the Z_h^N lattice a particle will jump to. This jump can be based upon a

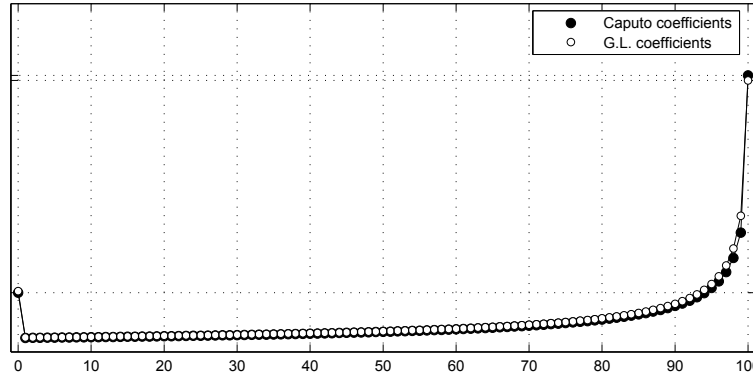


Figure 1: The weight w_m associated with the density u_j^m is plotted as a function of m for both the Caputo and Grünwald-Letnikov (G.L.) time-fractional derivatives and $\beta = 0.8$. The lower dotted horizontal line corresponds to the value of $w_0 \approx 0.005$ while the upper two dotted lines correspond to $w_n = c_1$ for both the Grünwald-Letnikov ($w_{100} = 0.8$) and Caputo derivatives ($w_{100} \approx 0.851$).

partitioning of the unit interval $\mathcal{P} = [0, 1)$ into two disjoint subintervals \mathcal{P}_1 and \mathcal{P}_2 such that $\mathcal{P} = \mathcal{P}_1 \cup \mathcal{P}_2$ where $\mathcal{P}_1 = [0, 1 - w_n)$ and $\mathcal{P}_2 = [1 - w_n, 1)$.

We will use a two-dimensional walk for illustration purposes. The random walk process begins by generating a uniformly distributed random number r in the unit interval and observing what subinterval (\mathcal{P}_1 or \mathcal{P}_2) it falls into. If $r \in \mathcal{P}_1 = [0, 1 - w_n)$, then the particle will do a *non-Markovian* jump, i.e. the jump will be determined by transition probabilities $w_m, m = 0, \dots, n - 1$. Otherwise, if $r \in \mathcal{P} = [1 - w_n, 1)$, then the particle will undergo a *Markovian* jump, i.e. the jump will be determined by transition probabilities p_k . In effect, the random walk interpretation presented here is a two-dimensional extension of the one-dimensional random walk interpretation given in [11].

4.2. Non-Markovian jumps. If $0 < \beta < 1$ and $r \in \mathcal{P}_1$, then the jump that the particle takes will be determined by $w_m, m = 0, \dots, n - 1$. Let $\mathcal{A} = \{\mathcal{A}_0, \mathcal{A}_1, \dots, \mathcal{A}_{n-1}\}$ be an n -element set such that $\mathcal{A}_i = w_i, i = 0, \dots, n - 1$. Furthermore, let the interval \mathcal{P}_1 be refined in the following way:

$$\mathcal{P}_1 = [\mathcal{B}_0, \mathcal{B}_1, \dots, \mathcal{B}_n),$$

such that $\mathcal{B}_0 = 0$ and $\mathcal{B}_j = \sum_{i=0}^{j-1} \mathcal{A}_i, j = 1, \dots, n$. If $r \in [\mathcal{B}_0, \mathcal{B}_1) = [0, w_0)$,

then the position of the particle at $t = t_{n+1}$ is given by $\mathbf{S}_{n+1} = \mathbf{S}_0$ (the origin). Otherwise, if $r \in [\mathcal{B}_{j-1}, \mathcal{B}_j)$, $j = 1, \dots, n$, then the particle will jump back to the position that it had visited at time $t = t_j$, i.e. $\mathbf{S}_{n+1} = \mathbf{S}_j$.

4.3. Markovian jumps when $\alpha = 2$. If $r \in \mathcal{P}_2 = [1 - w_n, 1)$ and $\alpha = 2$ then the jump will only be to adjacent lattice grid points. Let \mathcal{P}_2 be partitioned in the following manner:

$$\mathcal{P}_1 = [\mathcal{B}_0, \mathcal{B}_1, \dots, \mathcal{B}_5)$$

where $\mathcal{B}_0 = 1 - w_n$ and $\mathcal{B}_j = \mathcal{B}_0 + \sum_{i=0}^{j-1} \mathcal{A}_i$ ($j = 1, \dots, 5$). Here, $\mathcal{A} = \{\mathcal{A}_0, \mathcal{A}_1, \mathcal{A}_2, \mathcal{A}_3, \mathcal{A}_4\}$ where $\mathcal{A}_0 = w_n - 4\eta$ and $\mathcal{A}_i = \eta = \nu\tau^\beta/h^\alpha$, $i = 1, 2, 3, 4$. If $r \in [\mathcal{B}_0, \mathcal{B}_1)$, then the particle remains at the current position, otherwise if $r \in \{[\mathcal{B}_1, \mathcal{B}_2), [\mathcal{B}_2, \mathcal{B}_3), [\mathcal{B}_3, \mathcal{B}_4), [\mathcal{B}_4, \mathcal{B}_5)\}$ then the particle will move left, right, up or down, respectively, one lattice position.

4.3. Markovian jumps when DODE is given with the collection $\Lambda = \{\alpha_1, \dots, \alpha_M\}$, $\alpha_1 < \dots < \alpha_M < 2$. If $r \in \mathcal{P}_2 = [1 - w_n, 1)$ and $\Lambda = \{\alpha_1, \dots, \alpha_M\}$, then the jump will be determined by an *infinite* partition refinement of \mathcal{P}_2 . Let

$$\mathcal{A} = \{\mathcal{A}_0, \mathcal{A}_1, \dots\}; \quad \mathcal{P}_1 = [\mathcal{B}_0, \mathcal{B}_1, \dots)$$

such that $\mathcal{B}_0 = 1 - w_n$ and $\mathcal{B}_j = \mathcal{B}_0 + \sum_{i=0}^{j-1} \mathcal{A}_i$ ($j = 1, 2, \dots$). In this case, the set \mathcal{A} consists of all of the transition probabilities p_k , $k \in Z^2$, with $\mathcal{A}_0 = p_0$. If $r \in [\mathcal{B}_0, \mathcal{B}_1) = [1 - w_n, (1 - w_n) + p_0)$, then the particle will remain at the current position. Otherwise, if $r \in [\mathcal{B}_s, \mathcal{B}_{s+1})$, then there exists a unique $k = (k_1, k_2) \in Z^2$ associated with $s \in \mathbb{N}$ such that the particle will jump from \mathbf{S}_n to $\mathbf{S}_{n+1} = \mathbf{S}_n + (k_1h, k_2h)$.

5. Simulations

Our motivation of the numerical simulations presented here is to see how DODE simulations of biomolecular motion of particles on a cell surface differ from those based upon the classical Brownian motion. Although the DODE random walk models are described theoretically for multivariate case in N -dimensions, nevertheless all our simulations are conducted in the two dimensional case since we are interested in the diffusion of proteins on a cell membrane surface, which can be locally approximated by a two-dimensional membrane sheet. In [12], simulated particle motion is based upon the classical Brownian motion scenario (where $\alpha = 2$ and $\beta = 1$) in which the particle

is confined within cytoskeletal barriers (see Figure 2). In these single particle tracking studies, particle appears to be spatially and temporarily confined within *transient confinement zones*. Although the barriers are never directly observed, it is postulated that the cytoskeletal barriers are the reason for the transient spatial confinement of particle. In principle, DODE simulations provide an alternative explanation for the observed trajectories in single particle tracking studies that does not necessarily require the existence of cytoskeletal barriers to explain transient confinement.

In [12], the authors use the mean-squared-displacement formula $4a\tau = h^2$ in which the parameters a (the diffusion coefficient) , τ (the timestep) and h (the lattice width), respectively, are given using the following values: $h = 6$ nanometers and $\tau = 1\mu s$ (microseconds, or $\tau = 10^{-6}$ seconds). Since the mean-squared displacement formula implicitly assumes that

$$p_0 = 1 - 4a\frac{\tau^\beta}{h^\alpha} = 1 - 4a\frac{\tau}{h} = 0,$$

the diffusion coefficient is then computed as $a = h^2/(4\tau) = 9 \times 10^{-12}m^2/s$. To facilitate a comparison of our DODE simulations with the simulations of [12, 13], we will also use the same diffusion coefficient ($a_1 = \dots = a_M = a = 9 \times 10^{-12}m^2/s$) and the same lattice width ($h = 6$ nanometers). Using the fact that the transition probabilities sum to 1,

$$1 = \sum_{m=0}^{n-1} w_m + \sum_k p_k = (1 - w_n) + p_0 + \nu\tau^\beta q_0(h)$$

we can now solve for τ in terms of h, β, Λ and p_0 ,

$$\tau = \tau(h, \Lambda, \beta, p_0) = \left(\frac{c_1 - p_0}{\nu q_0(h)}\right)^{1/\beta} = \left(\frac{(2 - 2^{1-\beta}) - p_0}{\Gamma(2 - \beta)q_0(h)}\right)^{1/\beta}.$$

As in [12], we set $p_0 = 0$. However, due to the dependence of τ on Λ and β , the relative size of the timestep (from $\tau = 10^{-6}s$ in the case of $\alpha = 2$ and $\beta = 1$) will change as $\Lambda = \{\alpha_1, \dots, \alpha_M\}$ and β vary. Instead of fixing the simulations to have the same stepsize τ , we will fix the duration of the overall walk to be the same. Let T denote the overall duration of the random walk simulation. In all of our DODE simulations, T is set to $T = \frac{1}{30}$ seconds. This is equivalent to 1 frame at video rate where video rate is measured as 30 frames per second.

Figure 3 shows various Markovian DODE simulations ($\beta = 1$) across various values of components of Λ . The left, middle and right plots in the top row show DODE simulations with the single term $\alpha = \{2\}$, $\alpha = \{1.5\}$

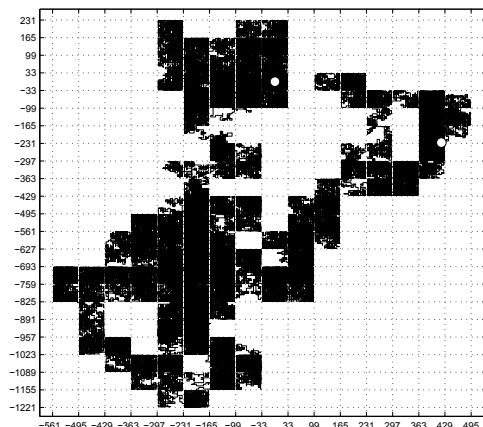


Figure 2: This random walk simulation depicts classical Brownian motion confined to rectangular cytoskeletal barriers. The parameters used in this simulation are as follows: $h = 6$ nanometers, $\tau = 10^{-6}s$ and $a = 9 \times 10^{-12}m^2/s$. The barriers are spaced out every 66 nanometers and the the probability of escape is $p = 0.01$ when a particle encounters a barrier.

and with two-terms with $\Lambda = \{1.5, 2\}$, respectively. The first two DODE simulations are actually monofractal DODE simulations with $M = 1$ while the last one ($\Lambda = \{1.5, 2\}$) is a multi-fractal case with $M = 2$. The large white dots indicate the first and last positions of the random walk and the starting position is always the origin $(0, 0)$. It is clear that for these DODE simulations with $\alpha \neq \{2\}$ that the particle travels much longer distances since the probability of jumping to faraway lattice sites is greater than what would be expected for $\alpha = 2$.

Figure 4 shows various non-Markovian DODE simulations ($\beta = 0.999$) using the same values of α as in Figure 3. The bottom plot in both Figures 3 and 4 show the plots on top row superimposed on one graph. The dark shaded lines correspond to Markovian jumps ($r \in \mathcal{P}_1$) while the white lines correspond to non-Markovian jumps ($r \in \mathcal{P}_2$). The frequency of the non-Markovian jumps are given by the size of the \mathcal{P}_1 interval. For $\beta = 0.999$, $\mathcal{P}_1 \approx [0, 1 - w_n) = [0, 0.00069339)$. Hence, the probability at every timestep of doing a non-Markovian jump is 0.00069339. The bottom plot in Figure 4 shows the superposition of all three non-Markovian DODE simulations on the same graph.

For Figure 5, we have non-Markovian DODE simulations for a fixed set of α values ($\Lambda = \{0.8, 1.3, 1.8\}$) with β varying. The left, middle and right plots correspond to $\beta = 0.999$, $\beta = 0.99$ and $\beta = 0.9$, respectively. The probability of taking a non-Markovian per timestep for these graphs is 0.00069339 (left), 0.0070 (middle) and 0.0718 (right). For example, roughly 7% of all jumps for the right subplot on the top row are non-Markovian jumps. The effect of decreasing β is clear: the overall distances that the particle traverses is decreased since motion is constrained by jumps to previously visited positions.

The average jump sizes associated with Figures 3, 4 and 5 are shown in Table 1. The numbers in the brackets before the colon correspond to the (Λ, β) pair used in the DODE simulation while the number after the colon corresponds to the average jump size. For the non-Markovian walks, the average jump length is larger when, for a fixed set of α values, β is decreased from 1. This is a consequence of the non-Markovian nature of the random walks for $0 < \beta < 1$. Since the particle is allowed to jump back to any previously visited position, the jump size can be quite large if the previously visited position was spatially remote from the particle's current position (see Figure 5). In particular, in Figure 1, the probability of the particle to jump back to the origin is disproportionately larger than for other previously visited sites. In Figures 4 and 5, one can observe evidence of this phenomenon.

	Left Plot	Middle Plot	Right Plot
Figure 3	(2,1): 6.0000	(1.5,1): 10.9770	({.5,2},1): 7.3320
Figure 4	(2,0.999): 6.0038	(1.5,0.999): 11.0707	({1.5,2},0.999): 7.3593
Figure 5	({0.8,1.3,1.8},0.999): 17.0328	({0.8,1.3,1.8},0.99): 17.1663	({0.8,1.3,1.8},0.9): 19.8946

Table 1: This table reports the average jump size (after the colon) for all of the DODE simulations in Figures 3, 4 and 5. The numbers before the colon indicates values of the (Λ, β) -pair used in the DODE simulation.

6. Conclusion

In this paper we constructed the random walk simulation model based on the so called distributed order differential equations. Analyzing the obtained results and comparing them with the classic Brownian motion and other simulations based on the one-term (monofractal) fractional order differential equations, we can make the following conclusion. Qualitatively,

the DODE simulations provide a richer repertoire of motion, compared to monofractal walks when $M = 1$. We remark that numerically this model corresponds to the explicit scheme (19), which can be considered as a generalization of the classic finite difference schemes. The obtained schemes are stable under some conditions, which we are going to report in another paper. One of the features of the represented model is that, macroscopically, the DODE trajectories tend to cluster together more often than the monofractal walks. The clustering is even more pronounced when the motion is non-Markovian due to the memory the particle has for previously visited positions. Moreover, one does not have to hypothesize the existence of barriers to explain why a particle appears trapped in a transient confinement zone or hops large distances. The clustering of trajectories and large jumps are a natural consequence of the DODE random walk model. However, when the motion is non-Markovian, the particle has a strong propensity to jump back to the origin, a consequence of the disproportionately large weight w_0 associated with u_j^0 . While jumping back to previously visited 'compartments' is observed for experimentally observed single particle tracking data [13], one does not experimentally observe molecules jumping back from its current position to the starting point. Nonetheless, the DODE random walk models closely resemble the data from single particle tracking experiments of molecules moving on cell membranes [12, 13]. This is not surprising since the motion of biomolecules on the cell surface occurs in a very heterogeneous environment.

Acknowledgment. This paper is partially supported by NIH grant P20 GMO67594.

References

- [1] R.L. Bagley, P.J. Torvic, On the existence of the order domain and the solution of distributed order equations I, II. *Int. J. Appl. Math.* **2** (2000), 865-882, 965-987.
- [2] J. Bouchaud, A. Georges, Anomalous diffusion in disordered media: Statistical mechanisms, models and physical applications. *Physics Reports* **195** (1990), 127-293.
- [3] M. Caputo, Linear models of dissipation whose Q is almost frequency independent. II. *Geophys. J. R. Astr. Soc.*, **13** (1967), 529-539.
- [4] M. Caputo, Distributed order differential equations modeling dielectric induction and diffusion. *Fract. Calc. Appl. Anal.* **4** (2001), 421-442.

- [5] A.V. Chechkin, R. Gorenflo, I.M. Sokolov, V. Gonchar, Distributed order time fractional diffusion equation. *Fract. Calc. Appl. Anal.* **6** (2003), 259-279.
- [6] M. Ciesielski and J. Leszczynski, Numerical simulations of anomalous diffusion. In: *Computer Methods in Mechanics, June 3-6, 2003, Gliwice, Poland*.
- [7] K. Diethelm, N.J. Ford, Numerical solution methods for distributed order differential equations. *Fract. Calc. Appl. Anal.* **4** (2001), 531-542.
- [8] M. Edidin, Lipid microdomains in cell surface membranes. *Curr. Opin. Struct. Biol.* **7** (1997), 528-532.
- [9] R.N. Ghosh, W.W. Webb, Automated detection and tracking of individual and clustered cell surface low density lipoprotein receptor molecules. *Biophys. J.* **66** (1994), 1301-1318.
- [10] R. Gorenflo, Yu. Luchko, S. Umarov, On the Cauchy and multipoint problems for partial pseudo-differential equations of fractional order. *Fract. Calc. Appl. Anal.* **3**, No 3 (2000), 249-277.
- [11] R. Gorenflo, F. Mainardi, D. Moretti, G. Pagnini and P. Paradisi, Discrete random walk models for space-time fractional diffusion. *Chemical Physics* **84** (2002), 521-541.
- [12] K. Ritchie, X.-Y. Shan, J. Kondo, K. Iwasawa, T. Fujiwara, A. Kusumi, Detection of non-Brownian diffusion in the cell membrane in single molecule tracking. *Biophys. J.* **88** (2005), 2266-2277.
- [13] K. Suzuki, K. Ritchie, E. Kajikawa, T. Fujiwara, A. Kusumi, Rapid Hop diffusion of a G-protein-coupled receptor in the plasma membrane as revealed by single-molecule techniques. *Biophys. J.* **88** (2005), 3659-3680.
- [14] F. Liu, S. Shen, V.Anh, I. Turner, Analysis of a discrete non-Markovian random walk approximation for the time fractional diffusion equation. *ANZIAM J.* **46** (2005), C488-C504.
- [15] C.F. Lorenzo, T.T. Hartley, Variable order and distributed order fractional operators. *Nonlinear Dynamics*, **29** (2002), 57-98.
- [16] M. Meerschaert, P. Scheffler, Limit theorems for continuous time random walks with slowly varying waiting times, *Statistics and Probability Letters* **71**, No 1 (2005), 15-22.
- [17] M. Meerschaert, P. Scheffler, *Limit Distributions for Sums of Independent Random Vectors. Heavy Tails in Theory and Practice*. John Wiley and Sons, Inc, New York (2001).

- [18] R. Metzler, J. Klafter, The random walk's guide to anomalous diffusion: a fractional dynamics approach. *Physics Reports* **339** (2000), 1-77.
- [19] S.G. Samko, A.A. Kilbas, O.I. Marichev, *Fractional Integrals and Derivatives: Theory and Applications*. Gordon and Breach Science Publishers, New York and London (1993).
- [20] M. Saxton, Anomalous Subdiffusion in Fluorescence Photobleaching Recovery: A Monte Carlo Study. *Biophys. J.*, **81**, No 4 (2001), 2226-2240.
- [21] M.J. Saxton, K. Jacobson, Single-particle tracking: applications to membrane dynamics. *Ann. Rev. Biophys. Biomol. Struct.*, **26** (1997), 373-399.
- [22] V.V. Uchaykin, V.M. Zolotarev, *Chance and Stability. Stable Distributions and their Applications*, VSP, Utrecht (1999).
- [23] S. Umarov, R. Gorenflo, On multi-dimensional symmetric random walk models approximating fractional diffusion processes. *Fract. Calc. Appl. Anal.* **8** (2005), 73-88.
- [24] S. Umarov, R. Gorenflo, The Cauchy and multipoint problem for distributed order fractional differential equations. *ZAA* **24** (2005), 449-466.
- [25] S. Umarov, S. Steinberg, Random walk models associated with distributed fractional order differential equations. In: *High Dimensional Probability*, IMS Lecture Notes - Monograph Ser. **51** (2006), 117-127.
- [26] G. Zaslavsky, Chaos, fractional kinetics, and anomalous transport. *Physics Reports* **371** (2002), 461-580.

† *Department of Mathematics and Statistics*
The University of New Mexico
 1 *University of New Mexico, MSC03-2150 Humanities Bldg # 81*
Albuquerque, New Mexico 87131, USA

‡ *Department of Pathology*
The University of New Mexico
Albuquerque, New Mexico 87131, USA

Received: June 20, 2006

* *Department of Mathematics and Mechanics*
The National University of Uzbekistan, Tashkent, UZBEKISTAN

e-mails:

andriese@math.unm.edu, sabir@math.unm.edu, stanly@math.unm.edu

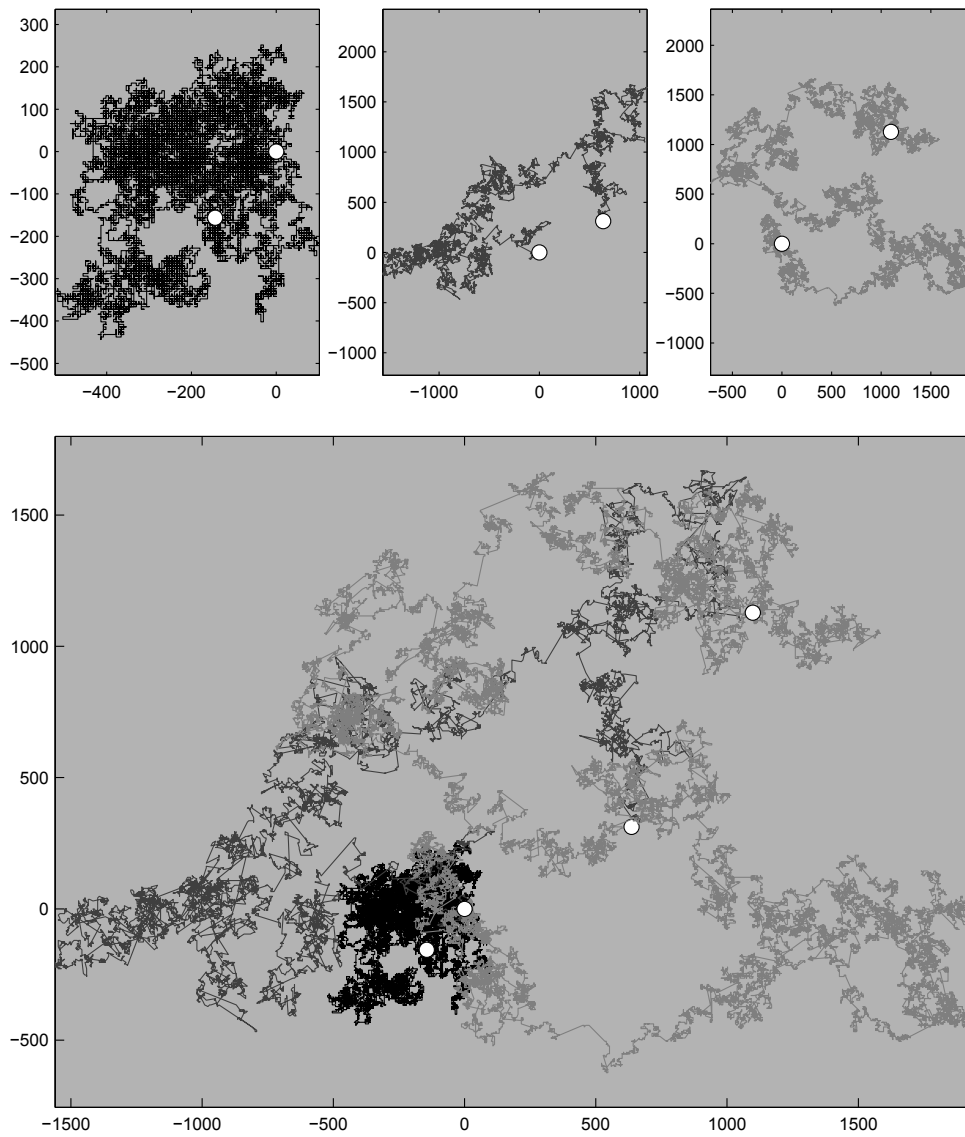


Figure 3: The first three subplots in the top row correspond to Markovian DODE simulations ($\beta = 1$) with different values of α : $\alpha = 2$, $\alpha = 1.5$ and $\Lambda = \{1.5, 2\}$ for the left, middle and right plots. The bottom plot superimposes all of the top three simulations on one graph.

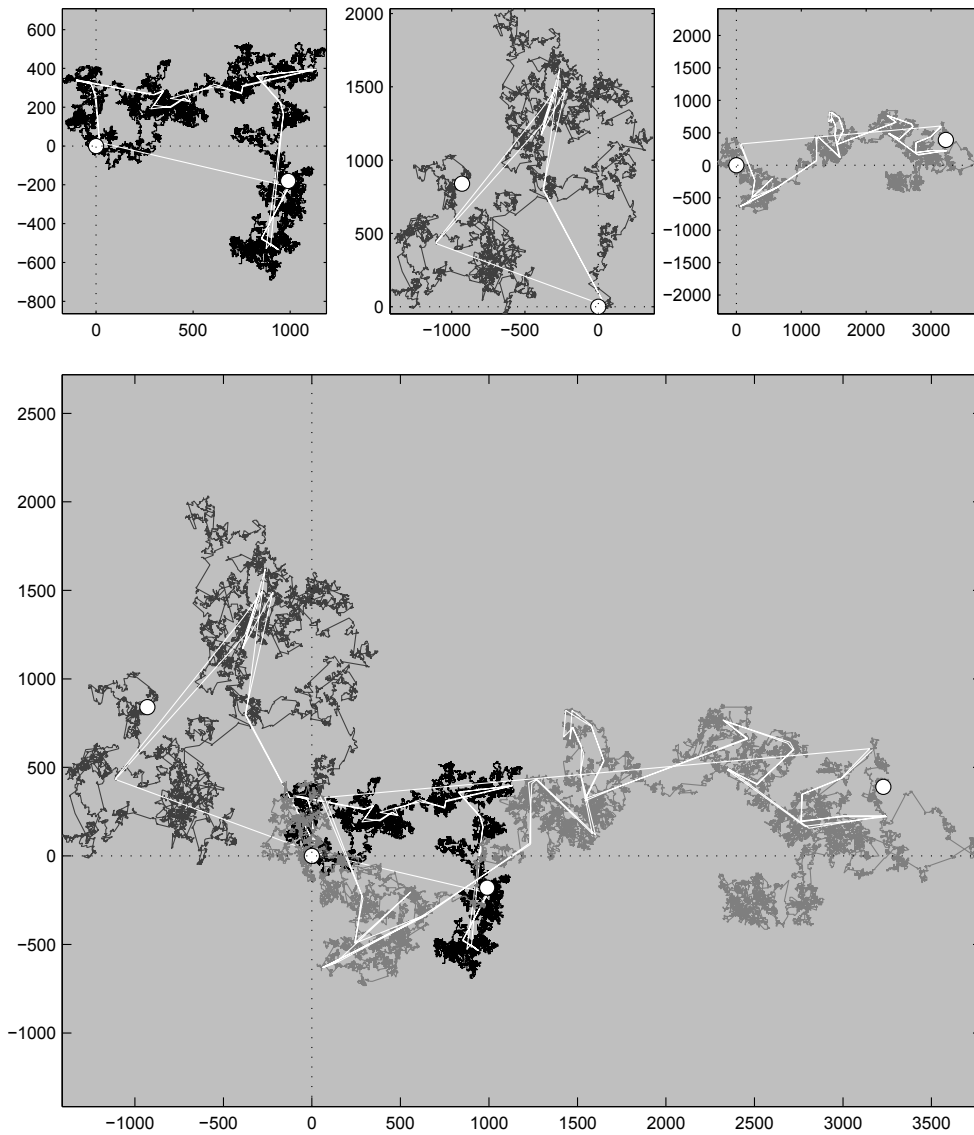


Figure 4: The first three subplots in the top row correspond to non-Markovian DODE simulations ($\beta = 0.999$) with different values of α : $\alpha = 2$, $\alpha = 1.5$ and $\Lambda = \{1.5, 2\}$ for the left, middle and right plots. The dark shaded lines correspond to non-Markovian walks while the white lines indicate non-Markovian jumps to previously visited positions. The bottom plot superimposes all of the top three simulations on one graph.

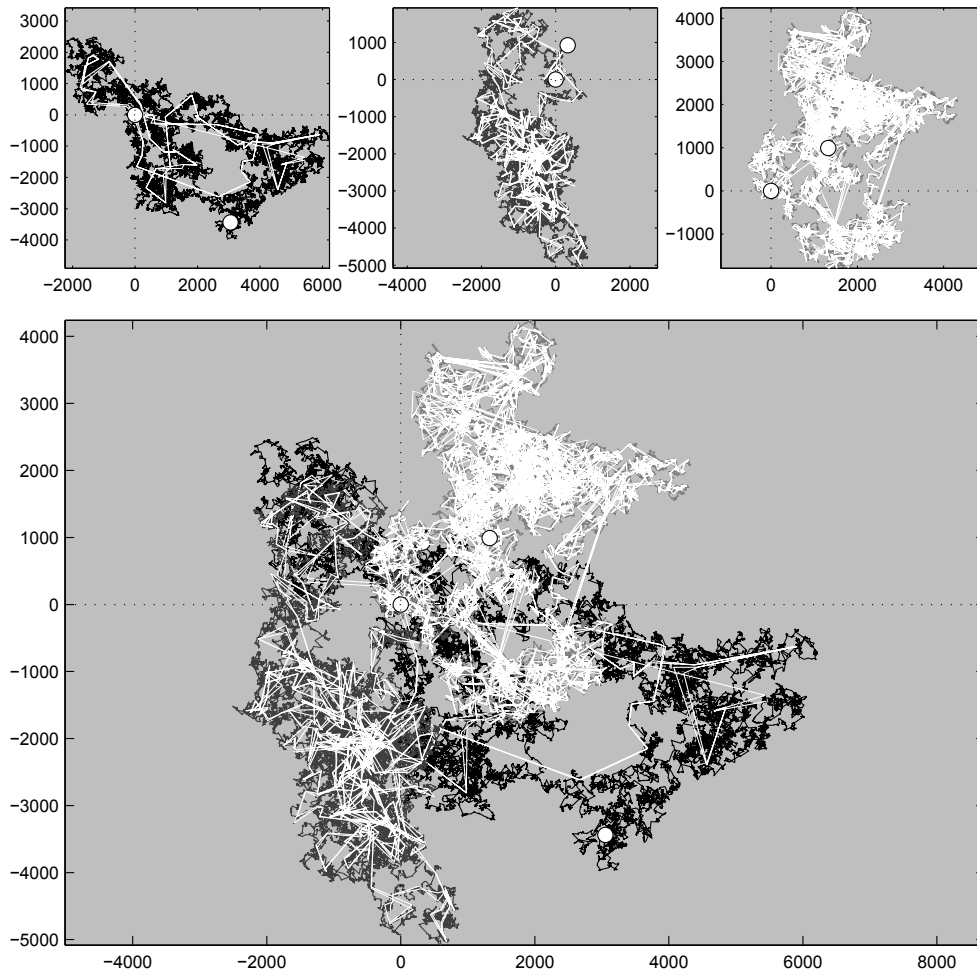


Figure 5: The first three subplots in the top row correspond to non-Markovian DODE simulations with $\Lambda = \{0.8, 1.3, 1.8\}$ and different values of β : $\beta = .999$, $\beta = .99$ and $\beta = .999$ for the left, middle and right plots. The dark shaded lines correspond to non-Markovian walks while the white lines indicate non-Markovian jumps to previously visited positions. The bottom plot superimposes all of the top three simulations on one graph.